Faraday Discussions

RSC Publishing

Cite this: *Faraday Discuss.*, 2013, **166**, 181

PAPER

View Article Online
View Journal | View Issue

Peptide nanofibres as molecular transporters: from self-assembly to *in vivo* degradation

Mariarosa Mazza,[ab] Avnish Patel,[a] Ramon Pons,[c] Cyrill Bussy[ab] and Kostas Kostarelos*[ab]

Received 17th June 2013, Accepted 15th July 2013
DOI: 10.1039/c3fd00100h

Peptide nanofibres (PNFs) have gained increasing interest as engineered biomaterials for drug delivery and tissue repair because of the versatility in design they offer through the self-assembly of amphiphilic peptide molecules. Their self-assembly is governed by hydrophobic interactions and hydrogen bonds between peptide sequences able to form β-sheets. In this report, we describe the self-assembly of PNFs by using palmitoyl-peptide molecules containing two different cationic amino acid sequences and offer a description of the nanofiber physicochemical characteristics. The structural degradation of these PNFs in physiologically-relevant media was evaluated experimentally and two mechanisms are proposed. We also piloted the tracking of PNFs intracellularly *in vitro*, upon interaction with primary neuronal cultures, and intracranially *in vivo*, after stereotactic administration deep within the brain using two types of fluorescent labelled PNFs. Overall, the self-assembled PNFs were seen to internalise within neurons and be removed or degrade in the brain. Further work is needed to determine the utility of such PNFs as molecular transporters within neuronal tissue.

Introduction

Peptide nanofibres (PNFs) are high axial ratio nanosized structures mimicking the size and shape of various naturally occurring nanoparticulate objects, *i.e.* viral capsids, actin cytoskeletons, and amyloid fibrils. PNFs can be formed by the self-assembly of peptides and peptide amphiphiles as self-assembly is a thermodynamically favourable event in aqueous environments. PNFs are versatile supramolecular architectures with potential as molecular transporters. Their building blocks can be designed to possess different functionalities resulting in chemical and physical properties tailored to specific needs.

[a]*UCL School of Pharmacy, University College London, Brunswick Square, London WC1N 1AX, UK. E-mail: k.kostarelos@ucl.ac.uk*

[b]*School of Medicine & National Graphene Institute, Faculty of Medical & Human Sciences, The University of Manchester, AV Hill Building, Manchester M13 9NT, UK*

[c]*Institut de Química Avançada de Catalunya, IQAC-CSIC, Jordi Girona 18–26, 08034 Barcelona, Spain*

The rational design of PNFs has to take into account several parameters that will influence the formation of high axial ratio nanostructures. Stupp and co-workers have designed many peptide amphiphiles having a palmitic moiety attached to the N-terminus of the peptide sequence conferring a surfactant-like architecture to the molecules. The same strategy has been adopted in this work enabling peptide self-assembly into nanofibres. Similar nanofibres have found a wide range of applications as biomaterials for tissue engineering.[1,2] Zhang and co-workers have developed peptide amphiphiles that are made of amino acids by alternating alanine residues in such a way that they pack with inter-digitated hydrophobic interactions in a similar fashion as occurs for alanine sequences in silk fibroin.[3,4] Other classes of peptide amphiphiles have been synthesized by varying the length of the alkyl chain.[5–7]

At the molecular level, parameters that need fine tuning in order to achieve the formation of PNFs include the hydrophobic domain, the hydrophilic block and a linker region of β-sheet forming peptides. The hydrophobic block can be represented by hydrophobic amino acids or alternatively a hydrophobic tail, often being represented by long acyl chains. The hydrophilic block is a sequence of basic or/and acid amino acids, often embedded within a biologically active peptide sequence. The linker region of β-sheet forming peptides contributes to the formation of elongated structures *versus* spherical micelles that most surfactant would form by self-assembling. Furthermore, the presence of aromatic side chain amino acids can determine the formation of cylindrical, ribbon like, twisted single or multiple fibres *via* the formation of π–π stacking. All of these parameters can give rise to a combination of factors that will influence the physicochemical characteristics of the resulting fibres as well as the interactions between nanofibers and other biological constituents.

In this work we report the formation of PNFs by two peptide molecules with emphasis on the structural disassembly of the nanofibres in physiological environments, as a result of the interaction between nanofibers and enzymes with possible degradation activities. We observed the self-assembly and characterized the PNFs formed. Their internalization within primary neuron cultures was determined by fluorescence microscopy. The *in vivo* localisation and structural stability of the PNFs were investigated following stereotactic administration in the brain parenchyma non-invasively using an IVIS camera.

Materials and methods

Preparation of PNFs

Peptides (palmitoyl-GGGAAAR and palmitoyl-GGGAAAKRK) were custom-made by Peptide Synthetics (Cambridge, UK) as freeze-dried powders at 95% purity. PNFs were prepared from a dispersion of 1 mg mL^{-1} peptide amphiphile in 5% dextrose (pH = 6.4) filtered through a 0.22 micron Millipore membrane filter. The final pH of the samples was 3.9–4.0, as both K and R are basic residues (R $pK_a = 12$; K $pK_a = 10.4$)[8] and thus bear a positive charge on the ionisable groups of the side chain. The dispersions were subject to 5 min of probe sonication at 20% of the maximum amplitude alternated with pulsed sonication of 20 s each.

Preparation of fluorescent labelled PNFs

PNF conjugation with fluorescent probe VivoTag 680. VivoTag 680 XL (absorbance at 688 ± 5 nm; Perkin Elmer) was reconstituted with 1 mL DMSO. A 1 mg mL^{-1} suspension was made using the freeze-dried peptide and phosphate buffered saline. This suspension was transferred into an amber Eppendorf tube to protect it from light. 50 μL of 1 M sodium bicarbonate and 2 μL of VivoTag 680 XL in DMSO were added. The tubes were maintained under constant agitation in a Tissuelyser (Qiagen) and set to oscillate 15 times per second for 2 h. The suspension was then centrifuged at 12 000 rpm for 4 min. The supernatant which contained unreacted dye was removed and discarded. The pellet was resuspended in 500 μL of distilled water which was filter sterilised by a 0.22 μm cellulose acetate syringe filter. The tubes were then centrifuged at 12 000 rpm for 4 min after which the supernatant was removed along with any remaining unreacted dye. The pellet was finally resuspended in filter sterilised dextrose 5% (w/v) giving a final concentration of 1 mg mL^{-1}. The prepared samples were then bath sonicated for 5 min using the pulse function, 15 s on and 5 s off. The samples were stored at 4 °C until needed.

Labelling PNFs non-covalently with Nile Red. An ethanol solution of Nile Red (1 mg mL^{-1}) was added dropwise to PNFs (1 mg mL^{-1}) in 5% dextrose during the probe sonication step to obtain a final v/v ratio of 1 : 9. The excess ethanol was eliminated by solvent evaporation while stirring the suspension overnight.

Transmission electron microscopy

TEM was performed using a Phillips Biotwin CM 210 electron microscope. 1% uranil acetate was used to counterstain the PNFs. For the degradation experiments 90 μL of either MEM, 0.05% trypsin–EDTA or rat plasma–PBS (1 : 1) was vortex mixed with 10 μL of PNFs in 5% dextrose. The samples were placed in a shaking incubator at 37 °C. Each sample was imaged at the following time points: 0, 0.5, 24, 48 h and after two weeks of incubation. The samples were prepared by transferring 10 μL onto a 300 grid copper mesh, and the drop was allowed to adsorb on top of the mesh for 10 s, after which the excess was wicked off using the edge of a filter disc. Uranyl acetate 1% (w/v) was used as a negative contrast agent, and was applied to the mesh, allowed to stand for approximately 5 s and then removed using the edge of a filter disc. The copper grid was then loaded for imaging. PNF lengths were measured for each time point using Image J to perform the semiquantitative image analysis.

Small angle X-ray scattering

Small-angle X-ray scattering (SAXS) measurements were carried out using a S3-MICRO (Hecus X-ray systems GMBH Graz, Austria) coupled to a GENIX-Fox 3D X-ray source (Xenocs, Grenoble), which provided a detector focused X-ray beam with a $\lambda = 0.1542$ nm Cu Kα-line with more than 97% purity and less than 0.3% Kα. Scattering of the transmission was detected using a PSD 50 Hecus. Temperature was controlled by means of a Peltier TCCS-3 Hecus. The samples were inserted in a flow-through glass capillary 1 mm diameter with 20 μm wall thickness. The SAXS scattering curves are shown as a function of the scattering vector modulus,

$$q = \frac{4\pi}{\lambda} \cdot \sin\frac{\theta}{2} \quad \text{(eq. 1)}$$

where θ is the scattering angle. The q values with our setup ranged from 0.08 nm^{-1} to 6.0 nm^{-1}. The system scattering vector was calibrated by measuring a standard silver behenate sample. Because of the use of a detector focused small beam (300 × 400 μm full width at half maximum) the scattering curves were mainly smeared by the detector width. This mainly produced a widening of the peaks without a noticeable effect on the peak position. The scattering curves for liquid samples have been background subtracted and put onto an absolute scale by comparison with the scattering of a water sample.[9,10]

The instrumentally smeared experimental SAXS curves were fitted to numerically smeared models for the beam size and detector width effects. A least squares routine based on the Levenberg–Marquardt scheme was used. Spherical and cylindrical models were fitted using two shell models.[11,12]

Degradation in plasma measured using UV-vis

Fluorescently labelled KRK PNFs were incubated in rat plasma–PBS (1 : 1), incubated at 37 °C under constant agitation in a water bath. UV absorbance measured using a Cary Bio 50 at different time points (0, 30 min, 1 h, 3 h, 6 h, 24 h, 2, 4, 7 and 10 days). The UV-vis spectrophotometer was set to measure the absorbance of light between 500 and 1000 nm, with data captured at 5 nm intervals. A blank was used to set a baseline before measuring the samples. After time 0 all samples, including blanks, were placed into a shaking water bath at 37 °C. All measurements were performed in a black 6Q quartz cuvette (Starna Scientific Ltd) with a path length of 1 cm. KRK PNFs were quantified by a mean calibration curve. All samples were measured in triplicate.

Cell uptake of PNFs

Primary neuronal cell cultures. Cell culture reagents (PBS, HBSS, trypsin, foetal bovine serum, DMEM:F12, neurobasal, B27, antibiotics) were purchased from Gibco (Life Technologies, UK). Neuron enriched cell cultures were prepared with hippocampus extracted from E16–E18 Wistar foetal rat brains (standard Witschi stages 33–34). Hippocampal tissue pieces were dissociated to single cell suspensions by trypsinization followed by mechanical trituration in Ca^{2+}/Mg^{2+} free HBSS solution. After determination of the number of live cells, 50 000 cells per well were plated onto a poly-D-lysine (50 μg ml^{-1}) coated glass bottom 8 well chamber slide (Millicell EZ SLIDE, Merck-Millipore) with DMEM:F12 medium completed with 12% heat inactivated foetal bovine serum and incubated at 37 °C in a humidified 5% CO_2 incubator. After 12 h, the medium was changed to serum free Neurobasal Medium supplemented with B27, glutamine (0.5 mM), penicillin (100 U), and streptomycin (100 μg). B27 supplement was used as a means to reduce glial cells growth and to obtain a nearly pure neuronal cell culture. Cultures were incubated in a humidified 37 °C/5% CO_2 incubator for 10 days before experimentation. Half of the medium was changed every 3 days. Primary neurons were exposed to the PNF–Nile Red formulations for 24 hours and the fluorescence was recorded using a Zeiss Axiovision Fluorescence Microscope.

Intracranial injection in mice

All experiments were performed in accordance with the approved recommendations and policies of the UK Home Office (Animal Scientific Procedures Act 1986, UK). Athymic nude mice (8 weeks old, Harlan, UK) were used for the *in vivo* experiments. Anaesthesia was induced by inhalation of isoflurane. 1 μL of fluorescently labelled KRK PNFs (1 mg mL^{-1}) was injected intracranially using a stereotactic frame. The stereotactic coordinates were: 0.1 mm posterior to the bregma, 2.3 mm to the right of the midline and 3 mm below the surface of the brain to target the caudate–putamen area of the brain. During surgical procedures, the animals were oxygenated and heated to ensure a 37 °C rectal temperature. After recovery, the animals were returned to their cages.

IVIS imaging

The fluorescence signal from the KRK PNFs labelled with VivoTag 680 XL in the brain was measured using an IVIS Lumina fluorescent imager (Caliper Life Sciences) with excitation at 675 nm and emission filter sets 700–840 nm.

Results and discussion

PNFs form as a result of the self-assembly of amphiphilic peptides. Although self-assembly is a thermodynamically favourable process, the time for the formation of these supramolecular structures has been shown to vary, from days to weeks for similar designer peptides and the nanofibril formation can take days or weeks to get to completion. It was recently reported that upon dissolution in ultrapure water of a hexapeptide amphiphile bearing aromatic side chain groups, short twisted bilayer ribbon segments were observed to be the dominant morphology after only 30 s, which then elongate on the time scale of minutes, and finally transform into helical ribbons over the course of weeks.[13,14] Under the same conditions, a similar peptide lacking aromatic side chains was shown to form cylindrical nanoparticles and not undergo any transition over a period of weeks.[14] Thus self-assembly may not only occur over a relatively long time, resulting in nanofibre formation, but there may also be a transition through metastable nanostructures before maturation into the equilibrated morphology. For such reasons, here we used a fast bottom approach to self-assembly for the preparation of PNFs. By employing probe sonication we reduced to a few minutes the time needed for the self-assembly process to take place. As previously reported by Mazza *et al.*,[15] this strategy can be employed to prepare an aqueous dispersion of short nanofibres below one micron (length range). PNFs were prepared by using two designer peptide amphiphiles in isotonic media (5% dextrose) at a concentration of 1 mg mL^{-1} and as a result of sonication we could observe by TEM the formation of cylindrical nanofibres as depicted in Fig.1A, C and D, F.

For both peptides under investigation in the present work we chose a palmitoyl chain as the hydrophobic block. Peptide and protein palmitoylation has been previously exploited to synthesize lipid derivatives[16] intended to increase membrane permeation. Unmodified peptides and proteins are generally poorly transported across biological membranes due to their hydrophilic nature, their high molecular weight and their instability to enzymatic degradation. Such palmitoylation strategies have been employed to increase the biological half-life of

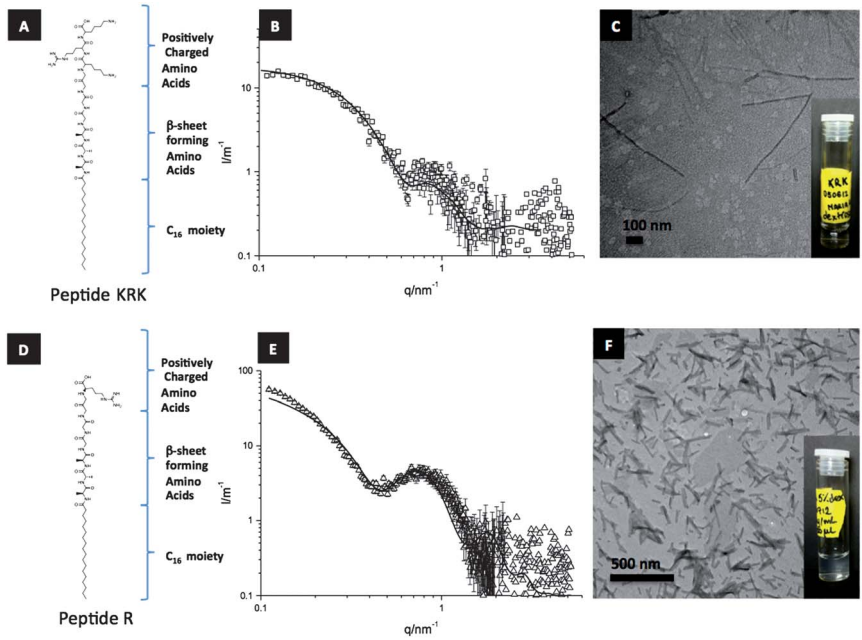

Fig. 1 (A) Molecular structure of peptide amphiphiles KRK. (B) SAXS pattern for KRK PNFs with the best fit of the core–shell cylindrical model. The error bars of the points at the right hand side have not been plotted for clarity. The scattering is smeared by the detector width and beam size. (C) Transmission electron micrograph of KRK PNFs (1 mg mL^{-1}) in 5% dextrose; the inset shows the physical appearance (clear solution) of the formulation after probe sonication. (D) Molecular structure of peptide amphiphiles R. (E) SAXS pattern for R PNFs with the best fit of the core–shell cylindrical model. The error bars of the points at the right hand side have not been plotted for clarity. The scattering is smeared by the detector width and beam size. (F) Transmission electron micrograph of R PNFs (1 mg mL^{-1}) in 5% dextrose; the inset shows the physical appearance (Tyndall effect) of the formulation after probe sonication.

therapeutic peptide molecules.[17] The covalent linkage of the C16 chain was designed to achieve a change in the physical properties of the peptide, enabling its self-assembly into high axial ratio nanostructures, as reported in the literature.[2,18,19] We then selected a short sequence of 6 amino acids able to form a β-sheet as a linker. Several reports have suggested that five is the minimum number of residues to include in a sequence in order to form a sequence capable of forming β-sheets for palmitoylated peptide amphiphiles.[20,21] Nevertheless, it is also known from the literature that β-sheet forming structures can arise from sequences as short as 2 amino acids, as in the case of Fmoc–diphenylalanine peptide self-assembly.[22,23]

The hydrophilic positively-charged block is the only segment that was different between the two structures and we believe the critical parameter determining the physico-chemical differences between the two PNF systems. The hydrophilic block in both peptide amphiphile structures was designed to be positively charged by the inclusion of basic amino acids. Charged PNFs can repel each other minimizing the aggregation in the system. Roberts *et al.*[24] have shown that for β-sheet forming peptides the net charge of the system, or charge modulus, has to be greater than 1 so that the electrostatic repulsion can prevent fiber aggregation,

independent of the sign of the charge. The choice of making the system positively charged rather than negatively charged was based on the consideration that most of the nanoparticles designed for intracellular delivery purposes should be positively charged, to favour the interaction with the moderately negatively charged cell surfaces.

One of the two peptides was assigned a positive charge by incorporating an arginine (R) at the C-terminus, while the other peptide was engineered by incorporating three peptides, lysine, arginine and lysine (KRK). The molecular structures of the two peptides are shown schematically in Fig. 1(A and D) and they will be referred to throughout the text as peptides R and KRK, respectively. In the case of peptide R, final PNFs with a modest positive charge were aimed for, while in the case of peptide KRK, highly positively charged PNFs were studied. Both peptides included in their sequence the highly basic residue arginine, that is often found in dense protein patches and is able to form bidentate hydrogen bonds as a consequence of the charge delocalization on the guanidinium group.[25] Oligopeptides incorporating an arginine headgroup have been reported to undergo self-assembly into nanosheets[26] and nanofibrils.[27]

After sonication we could observe that the PNF dispersion of the less positive peptide amphiphile (peptide R) was translucent, due to the Tyndall effect (inset in Fig. 1F). The PNF dispersion prepared with the KRK peptide was transparent (inset in Fig. 1C). We then studied the morphology of the PNFs by SAXS to characterize the shape and the dimensions of the nanostructures. Fig. 1B shows the scattering pattern of the KRK PNFs in 5% dextrose at 25 °C together with the best fit of a core–shell cylindrical model. There is a medium range shoulder centred at 0.9 nm^{-1} and an increase of intensity at small q.

The fitting of the core–shell model adequately captures the essence of the experimental scattering. The parameters of the fits correspond to 5.2 ± 0.6 nm for the outer radius and 4.4 ± 0.4 nm for the inner radius. According to the determined electron densities of the core and shell (306 e nm^{-3} for the core and 346 e nm^{-3} for the shell), there should be significant presence of high electron density atoms (nitrogen and oxygen as compared to the low electron density hydrocarbon chains) in the cores of the cylinders. The whole picture is consistent because, if only hydrocarbon chains were in the core, this should have a maximum radius of about 2.0 nm based on the palmitoyl chain length and the electron density of the core should be approx. 280 e nm^{-3}. If we account for the maximum length of the hydrophobic core as corresponding to the palmitoyl chain plus the hydrophobic amino acid chain, this corresponds to approx. 5.6 nm which is enough to be accommodated within the determined 4.4 nm. The length of the cylinders lies out of our SAXS window and we can only estimate a minimum length of 100 nm.

The Guinier analysis in the small q regime corresponds to only 7 nm radius for globular aggregates and the cylinder form of the Guinier analysis produces a 3.2 nm cylinder radius and 38 nm cylinder length. This could explain part of the difference with the R peptide amphiphile whose charge corresponds only to the terminal arginine group which at neutral pH should bear both positive and negative charges. The SAXS result is shown in Fig. 1E. In this case the intensity grows faster at small q and also the shoulder at intermediate q is more evident than for the case of KRK. This is partially due to stronger segregation of the hydrophilic and hydrophobic moieties of the peptide amphiphile. The cylinder

core radius corresponds to 0.8 ± 0.2 nm while the outer radius is similar to that of KRK, 5.2 ± 0.4 nm. The core electron density is 299 e nm^{-3} while the shell electron density is 342 e nm^{-3}. The cylinder length is also out of the observation window and can be estimated as more than 100 nm. In this case, the Guinier analysis produces an estimated globular radius of 32 nm (clearly excessive) and cylindrical estimates of 9 nm for the radius and 64 nm for the length of the PNFs, in agreement with the fitted values.[28]

Similar peptide amphiphile solutions have also been studied previously using SAXS. Long fibril-forming systems, as determined by optical techniques, tend to show q^{-1} behaviour at small q values while the presence or absence of shoulders at intermediate q values is determined by the specific contrast variation across the cylinder section. The q^{-1} behaviour at small q can also be obscured by the specific contrast variation, as shown by the fitting obtained for KRK or by interparticle effects.[29] The tendency to form cylindrical aggregates at low concentrations can be considered a property of peptide amphiphiles and is probably promoted by the presence of intermolecular hydrogen bonding. Indeed, the formation of micelles at low concentration of peptide amphiphiles has been demonstrated in both single chain[30] and gemini lipoaminoacid surfactants.[10]

The structure analysis performed using transmission electron microscopy shows that peptide R (Fig. 1F), could assemble into short PNFs with a rod-like stiff structure and a formulation resulting in a highly light-scattering suspension. Peptide KRK formed more flexible elongated nanofibres (Fig. 1C). Taken together, this information supports the hypothesis that surface charge is an important factor to be considered for the fabrication of PNFs that could be designed for the transport of various molecules.

Peptide nanofibres are commonly considered biodegradable because they consist of amphiphilic peptides and peptides that can be enzymatically degraded by endogenous peptidases *via* hydrolysis of the amidic bond formed between amino acids. Nevertheless, adjacent peptide amphiphiles can form H-bonds at the level of their β-sheet forming sequences.

We postulate that enzymatic degradation may occur in two different ways: a) the enzyme can dissociate the PNFs into smaller fragments, or b) the disassembly may occur from the two ends towards the centre, as the single peptide units are cleaved to result in the shortening of the PNFs (Fig. 4). In both cases, the enzymes can hydrolyse the peptidic bonds between two amino acids and break down each peptide amphiphile monomer into its amino acid constituents. Peptidases can cleave the amino acids either by hydrolysis of the amide bond starting from the N-terminus (aminopeptidases) or by hydrolysis from the C-terminus (carboxy-peptidases). In the two peptide amphiphiles the N-terminus was chemically modified *via* the attachment of the palmitoyl chain and these hydrophobic chains were packed to form the lipophilic core of these nanostructures, making this site not readily available to aminopeptidases. Furthermore the β-sheet forming peptides are involved in the formation of the H-bonds, also inaccessible to enzymes. The C-terminus will be available to enzymes, since it is part of the hydrophilic head group, exposed towards the aqueous environment. Carboxy-peptidases should be able to interact with the C-terminus and act to hydrolyse the amino acids.

To test this hypothesis we decided to study the PNF degradation as a function of UV absorbance by incorporation of a probe. We modified the peptides using

VivoTag 680 XL by the formation of an ester link between the amino group on the peptide side chains (K and R) of the basic amino acids and the N-hydroxysuccinimide of the probe molecule. The reaction with peptide R resulted in the formation of a highly hydrophobic peptide that precipitated into an insoluble product. This was due to the chemical modification of the basic R leading to the neutralization of its positive charge. Modification of peptide KRK was successful and the conjugate was well dispersed in 5% dextrose, thus PNFs were readily prepared using the sonication protocol.

The fluorescently labelled PNFs were incubated with plasma (plasma : PBS = 1 : 1) and the UV-vis absorbance measured to estimate the structural integrity over ten days (Fig. 2). There was an intensity decrease of about 10–15% in the first 6 days, and it was indicated that the structural integrity of the PNFs was reduced by 50% in 7 days and it reached about 33% after 14 days of incubation. At 21 days the absorbance was below the limit of detection, thus the value measured for the absorbance was not considered reliable. These data suggest that circulating peptidases present in plasma were able to metabolize the PNFs.

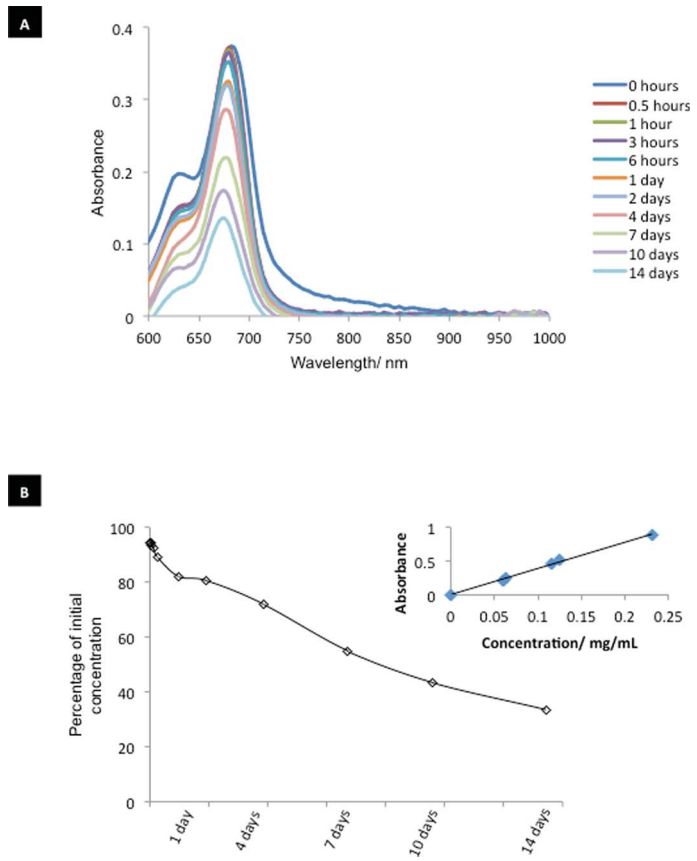

Fig. 2 UV-vis spectroscopy of KRK PNFs. Labelled KRK PNFs were incubated in rat plasma–PBS (1 : 1) and measured by UV absorbance. The percentage of intact fiber was measured by means of a calibration curve (inset).

The KRK PNFs were then incubated in 0.05% trypsin–EDTA. Trypsin was chosen as a model carboxypeptidase to test the hypothesis that they can degrade PNFs. Samples were imaged using TEM at different time points to observe any structural change and length variation that may occur during the enzymatic degradation process (Fig. 3A). 30 min post-incubation the PNFs had a stable structure. The semi-quantitative image analysis of the TEM images (Fig. 3B) shows that already after 24 h there is a reduction in the length of the nanofibres. There continues to be an overall reduction of the PNFs after 48 h with the size distribution widening, perhaps due to the coalescence of smaller fibres (Fig. 3A). At 14 days the PNFs were very hard to identify by TEM.

Previous studies have reported that peptide nanofibre gels designed to incorporate a proteolytic sequence incubated with collagenase IV in HEPES-buffered saline solution were completely degraded after one month.[31] Enzyme

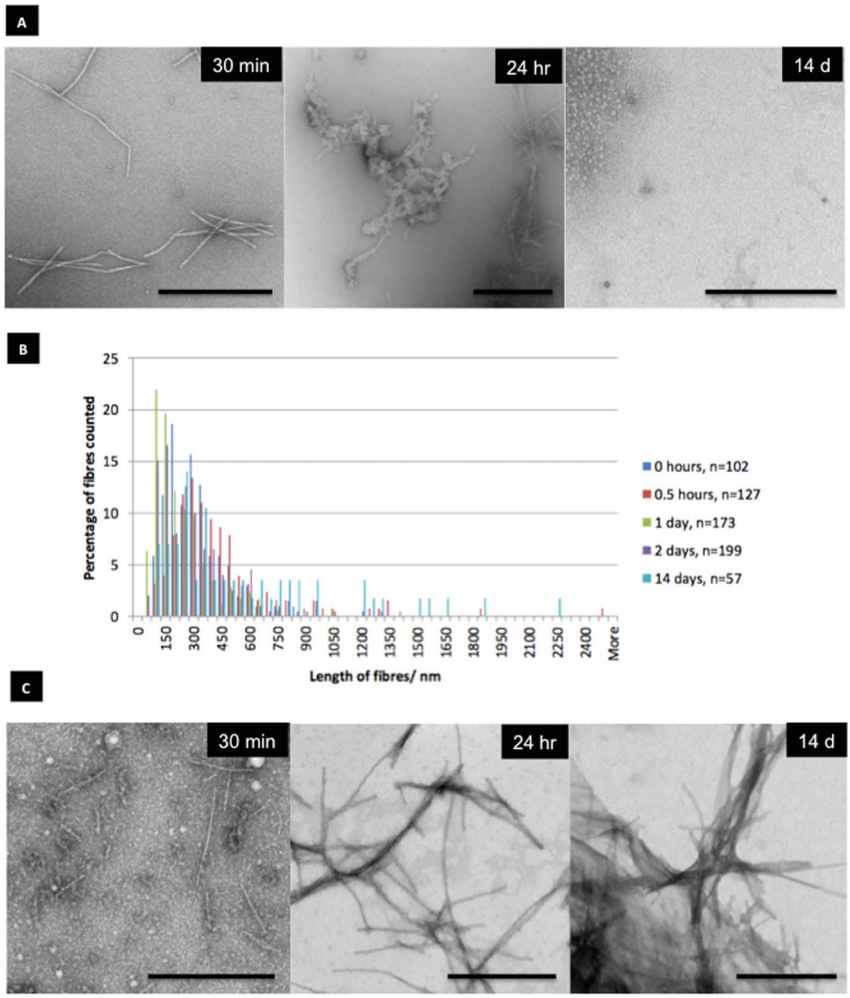

Fig. 3 Degradation of PNFs measured by TEM. (A) TEM images of KRK nanofibres incubated with 0.5% trypsin–EDTA; (B) semiquantitative analysis of the TEM images; (C) TEM images of KRK PNFs incubated with MEM (negative control). All scale bars = 500 nm.

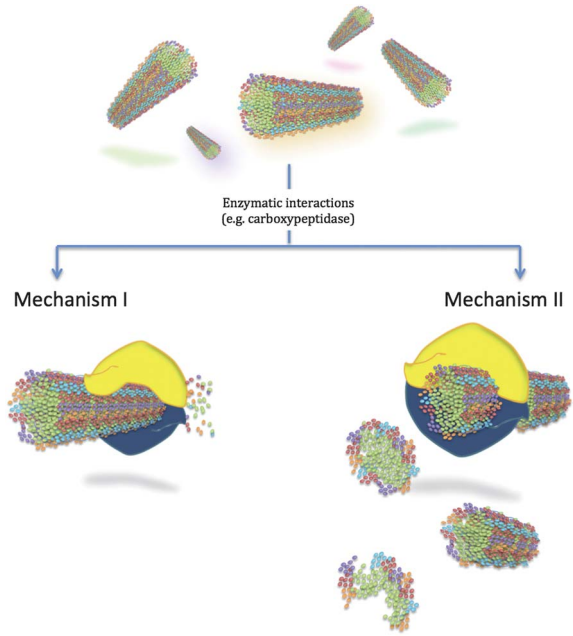

Fig. 4 Schematic depiction of two proposed mechanisms leading to PNF degradation. Degradation of PNF into its amino acidic components by peptidase. Mechanism I shows degradation of PNFs by cleavage of amino acids from the fibre ends towards the middle. Mechanism II shows degradation of PNFs into shorter nanofibres and formation of amorphous aggregates.

attack at multiple sites can also perturb the assembly into nanofibres and H-bond breaks can increase the molecular mobility of the peptides resulting in a more disordered packing. Furthermore, as the H-bonds are broken the sites for enzymatic degradation are less sterically hindered and amino acids can be cleaved easier. KRK PNFs were also incubated in cell culture media (MEM) that did not contain any enzyme. No signs of degradation were observed, however PNFs showed in cell media a tendency toward aggregation overtime (Fig. 3C). This could be attributable to a buffering effect of the ions present in the cell medium on the positive charges on the PNF surface and to electrostatic interactions with other amino acid constituents in the media. From these *in vitro* assays we could conclude that PNFs were structurally unstable in biological media that contained enzymes. Moreover, the enzyme-mediated disassembly process seemed to favour the mechanism II in Fig. 4, first evidenced by PNF length reduction, and then structural degradation.

We then investigated how KRK PNFs interacted with living cells. To study the cellular internalization, KRK nanofibers were labelled with Nile Red, an hydrophobic dye, encapsulated into the nanofiber hydrophobic core. This time a fluorescent dye not covalently linked to the PNF was preferred in order to leave the positive charges on the PNF surface free to interact with the cell surface. Then, the tagged nanofibers were incubated with cultured primary neurons isolated from the striatum of rat brains for 24 h and the cells were examined by light and fluorescence microscopy, as shown in Fig. 5A. The fluorescence signal in the cytoplasm of the primary neurons demonstrated that the interaction of the

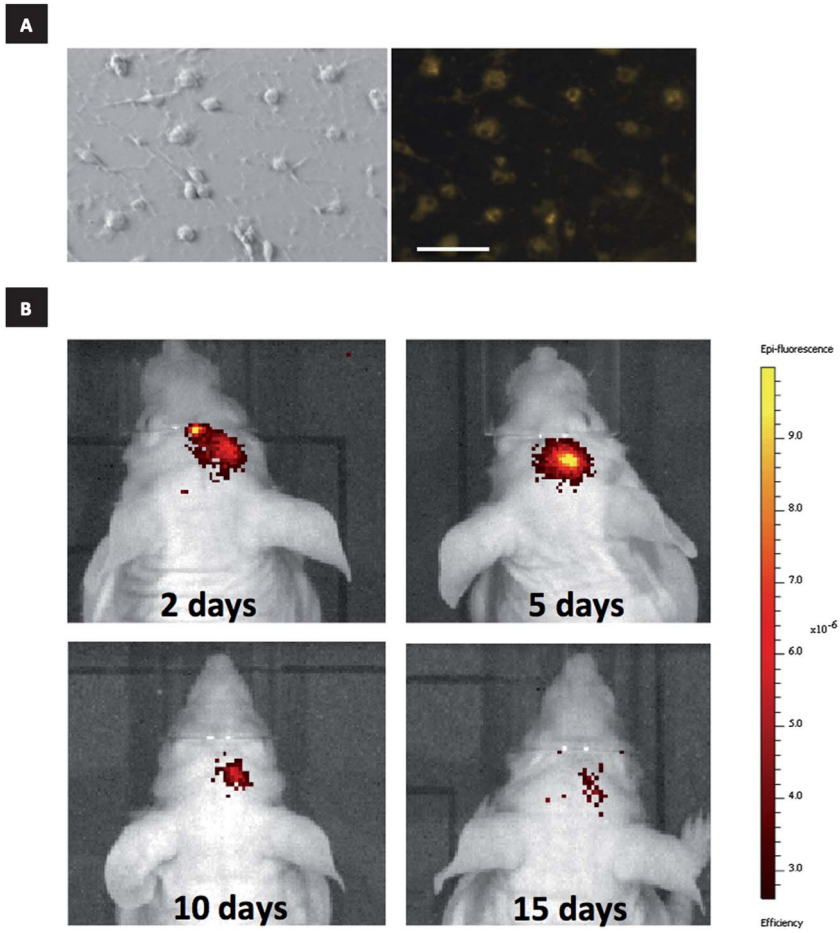

Fig. 5 (A) Cell internalization of KRK PNFs encapsulating Nile Red by primary neurons isolated from rat brain (scale bar = 50 μm); (B) residence time (days) of KRK PNFs fluorescently labelled with VivoTag 680 XL injected intracranially in the right brain hemisphere (caudate–putamen) in athymic nude mice, imaged with an IVIS Lumina camera at 675 nm.

positively charged PNFs with the cell surface results in internalization of the PNFs. The fiber shaped PNFs may offer an additional cell entrance gate by energy-independent internalisation mechanisms, similar to other high axial ratio nanostructures that have been previously described to pierce the plasma membrane.[32]

In this context, PNFs may offer the ideal platform as a nanocarrier because of the versatility with which they can be engineered. They can be employed as carriers for small hydrophobic molecules,[33] and at the same time potentially show more versatility as a fiber-shaped transporter. PNFs also seem to be degradable in biological environments, so we decided to perform a pilot *in vivo* degradability study. PNFs have been shown to be biocompatible scaffolds for neuronal differentiation[34] and have been investigated as carriers of bioactive molecules to the CNS.[15] However, PNFs structurally resemble in shape amyloid fibrils, misfolded

protein aggregates that are involved in a number of neuropathologies associated with neurodegeneration.[35]

For these reasons we decided to study the residence time of the PNFs injected directly in the brain parenchyma, as an initial step towards assessment of the safety of this approach for CNS therapeutic delivery. A variety of peptidases have been detected in the tissues of the CNS, some of these are membrane bound and others are soluble and exist in the highest concentration in the neural cell cytosol.[36] Carboxypeptidases are present in the brain and CSF[37] and are responsible for the enzymatic degradation of peptides starting from the C-terminus. We studied the residence time of the VivoTag 680 XL fluorescently labelled KRK PNFs after intracranial injection in the caudate–putamen of athymic nude mice.

The residence time of the PNFs in living animals (under anaesthesia) was measured by following the fluorescent signal using an IVIS fluorescence imaging camera. A strong fluorescent signal was observed for up to 1 week upon intracranial injection. Furthermore, it is worth noting that the signal remained located in the right hemisphere, in proximity to the site of injection. After 10 days the PNF fluorescent signal exhibited a considerable decrease and was further weakened after 15 days. This data suggests that the PNFs were removed or degraded in the brain parenchyma. Much further work should be performed in continuation of this pilot *in vivo* study.

Conclusions

This study has demonstrated that PNFs in suspension can be internalized by cells, and degraded overtime in enzyme containing biological fluids and possibly by enzymes expressed *in vivo*. We provided here some initial evidence that nanofibres may have a reduced risk of accumulation and prompt further exploration as transporters of therapeutic and diagnostic agents to the CNS.

Acknowledgements

This work was partially funded by the European Commission research programme FP7-NANOSOLUTIONS (FP7-NMP-2012-309329). RP acknowledges financial support from Generalitat de Catalunya (2009SGR1331), MINECO (CTQ2010-14897) and J. Caelles for the SAXS-WAXS service at IQAC, and technical support on the SAXS measurements.

References

1 H. Cui, M. J. Webber and S. I. Stupp, *Biopolymers*, 2010, **94**, 1.
2 J. D. Hartgerink, E. Beniash and S. I. Stupp, *Science*, 2001, **294**, 1684.
3 S. Vauthey, S. Santoso, H. Gong, N. Watson and S. Zhang, *Proc. Natl. Acad. Sci. U. S. A.*, 2002, **99**, 5355.
4 S. Zhang, D. M. Marini, W. Hwang and S. Santoso, *Curr. Opin. Chem. Biol.*, 2002, **6**, 865.
5 P. Forns, J. L. Lauer-Fields, S. Gao and G. B. Fields, *Biopolymers*, 2000, **54**, 531.
6 Y.-C. Yu, M. Tirrell and G. B. Fields, *J. Am. Chem. Soc.*, 1998, **120**, 9979.
7 X.-D. Xu, Y. Jin, Y. Liu, X.-Z. Zhang and R.-X. Zhuo, *Colloids Surf., B*, 2010, **81**, 329.
8 R. L. Thurlkill, G. R. Grimsley, J. M. Scholtz and C. N. Pace, *Protein Sci.*, 2006, **15**, 1214.
9 D. Orthaber, A. Bergmann and O. Glatter, *J. Appl. Crystallogr.*, 2000, **33**, 218.
10 L. Pérez, A. Pinazo, M. R. Infante and R. Pons, *J. Phys. Chem. B*, 2007, **111**, 11379.
11 R. Pons, M. Valiente and G. Montalvo, *Langmuir*, 2010, **26**, 2256.
12 J. S. Pedersen, *Adv. Colloid Interface Sci.*, 1997, **70**, 171.
13 E. T. Pashuck, H. Cui and S. I. Stupp, *J. Am. Chem. Soc.*, 2010, **132**, 6041.

14 E. T. Pashuck and S. I. Stupp, *J. Am. Chem. Soc.*, 2010, **132**, 8819.
15 M. Mazza, R. Notman, J. Anwar, A. Rodger, M. Hicks, G. Parkinson, D. McCarthy, T. Daviter, J. Moger, N. Garrett, T. Mead, M. Briggs, A. G. Schatzlein and I. F. Uchegbu, *ACS Nano*, 2013, **7**, 1016.
16 M. Foldvari, S. Attah-Poku, J. Hu, Q. Li, H. Hughes, A. B. Lorne and S. Kruger, *J. Pharm. Sci.*, 1998, **87**, 1203.
17 L. Yuan, J. Wang and W. C. Shen, *Eur. J. Pharm. Biopharm.*, 2008, **70**, 615.
18 Z. Yang, W. T. Huck, S. M. Clarke, A. R. Tajbakhsh and E. M. Terentjev, *Nat. Mater.*, 2005, **4**, 486.
19 I. W. Hamley, A. Dehsorkhi and V. Castelletto, *Langmuir*, 2013, **29**, 5050.
20 V. Castelletto, I. W. Hamley, J. Perez, L. Abezgauz and D. Danino, *Chem. Commun.*, 2010, **46**, 9185.
21 A. Dehsorkhi, I. W. Hamley, J. Seitsonen and J. Ruokolainen, *Langmuir*, 2013, **29**, 6665–6672.
22 C. Tang, A. M. Smith, R. F. Collins, R. V. Ulijn and A. Saiani, *Langmuir*, 2009, **25**, 9447.
23 A. M. Smith, R. J. Williams, C. Tang, P. Coppo, R. F. Collins, M. L. Turner, A. Saiani and R. V. Ulijn, *Adv. Mater.*, 2008, **20**, 37.
24 D. Roberts, C. Rochas, A. Saiani and A. F. Miller, *Langmuir*, 2012, **28**, 16196.
25 K. Zhao, U.-J. Choe, D. T. Kamei and G. C. L. Wong, *Soft Matter*, 2012, **8**, 6430.
26 I. W. Hamley, A. Dehsorkhi and V. Castelletto, *Chem. Commun.*, 2013, **49**, 1850.
27 I. W. Hamley, A. Dehsorkhi, V. Castelletto, J. Seitsonen, J. Ruokolainen and H. Iatrou, *Soft Matter*, 2013, **9**, 4794.
28 A. Pinazo, L. Perez, M. R. Infante and R. Pons, *Phys. Chem. Chem. Phys.*, 2004, **6**, 1475.
29 C. L. Pizzey, W. C. Pomerantz, B.-J. Sung, V. M. Yuwono, S. H. Gellman, J. D. Hartgerink, A. Yethiraj and N. L. Abbott, *J. Chem. Phys.*, 2008, **129**, 095103.
30 T. Imae, N. Hayashi, T. Matsumoto, T. Tada and M. Furusaka, *J. Colloid Interface Sci.*, 2000, **225**, 285.
31 H. W. Jun, V. Yuwono, S. E. Paramonov and J. D. Hartgerink, *Adv. Mater.*, 2005, **17**, 2612.
32 L. Lacerda, J. Russier, G. Pastorin, M. A. Herrero, E. Venturelli, H. Dumortier, K. T. Al-Jamal, M. Prato, K. Kostarelos and A. Bianco, *Biomaterials*, 2012, **33**, 3334.
33 S. Soukasene, D. J. Toft, T. J. Moyer, H. Lu, H. K. Lee, S. M. Standley, V. L. Cryns and S. I. Stupp, *ACS Nano*, 2011, **5**, 9113.
34 G. A. Silva, C. Czeisler, K. L. Niece, E. Beniash, D. A. Harrington, J. A. Kessler and S. I. Stupp, *Science*, 2004, **303**, 1352.
35 E. H. Koo, P. T. Lansbury, Jr and J. W. Kelly, *Proc. Natl. Acad. Sci. U. S. A.*, 1999, **96**, 9989.
36 A. Turner, in *Neuropeptides and their peptidases*, ed. A. Turner, Ellis Horwood, Chichester and Verlagsgesellschaft, 1987.
37 M. B. Segal, *Barriers and fluids of the eye and brain*, Macmillan, 1992.

